C. R. Mecanique 342 (2014) 671–691

Contents lists available at ScienceDirect

Comptes Rendus Mecanique

www.sciencedirect.com

A reduced simulation applied to the viscoelastic fatigue of polymers

Mohammad Hammoud [a,*], Marianne Beringhier [b], Jean-Claude Grandidier [b]

[a] Structure Dynamics Materials Group, Mechanical Department, School of Engineering, Lebanese International University, Mouseitbeh, Beirut, Lebanon

[b] Institut P′, Département "Physique et mécanique des matériaux", UPR CNRS 3346, ISAE–ENSMA, 86360 Chasseneuil-du-Poitou, France

ARTICLE INFO

Article history:
Received 23 March 2014
Accepted 28 July 2014
Available online 15 August 2014

Keywords:
PGD
Polymer
Viscoelastic
Internal variable
Relaxation
Model reduction

ABSTRACT

The paper extends the use of the PGD method to viscoelastic evolution problems described by a large number of internal variables and with a large spectrum of relaxation times. The internal variables evolution is described by a set of linear differential equations that involve many time scales. The feasibility and the robustness of the method are discussed in the case of a polymer in a non-equilibrium state under creep and cyclic loading. The relationships between different time scales (loading and internal variables) are also discussed.

1. Introduction

In order to model the behavior of materials, internal variables have to be introduced to correctly take into account dissipative phenomena [1–3]. This approach has proven its efficiency in viscoelasticity, viscoplasticity, plasticity and also continuum damage mechanics. The corresponding models are often based on differential equations to represent the kinetic evolution of microscopic phenomena. Except in the case of extended continuum mechanics [4,5], these internal variables are local and integrated at each integration point in the classical Finite-Element Method (FEM). For most of these models, the number of internal variables is limited and reasonable, but it may become very large in the context of viscoelasticity. From a numerical point of view, the simulations can be performed for many situations. But, if we imagine simulations with hundreds or thousand cycles (fatigue), the computation time can be prohibitive.

A typical example is the viscoelasticity of polymers, described by a continuous distribution of the relaxation times. Cunat has demonstrated in 1991 [6] that a minimal number of relaxation times and consequently internal variables are needed to correctly describe the viscoelastic behavior with a discrete point of view. Usually, 50 relaxation times are used to approximate a discrete spectrum spread over six decades [7]. The evolution law associated with each internal variable consists in a differential equation with respect to time. To simulate this behavior, we have to solve simultaneously the mechanical equilibrium equation and 50 evolution laws.

From a numerical point of view, the use of the classical FEM leads to a large computation time linked to the incremental scheme, especially in the case of nonlinear differential equations. Namely, at each time step, we have to solve 50 equations

* Corresponding author. Tel.: +961 71 504 815.
E-mail addresses: mouhamad.hammoud@gmail.com (M. Hammoud), marianne.beringhier@ensma.fr (M. Beringhier), jean-claude.grandidier@ensma.fr (J.-C. Grandidier).

http://dx.doi.org/10.1016/j.crme.2014.07.008
1631-0721/

for each Gauss point. In the case of linear differential equations, analytical solutions allow a quick estimation of the evolution of the internal variables at each time step. Otherwise, if the differential equations are strongly nonlinear, their solving necessitates to consider another temporal scheme, for example an adaptive Runge–Kutta scheme [8]. These numerical issues are particularly adapted for long relaxation times. Indeed, it is efficient to solve creep and relaxation problems by combining an adaptive method for the resolution of a nonlinear behavior law at each Gauss point, with an algorithm that optimizes the global step time. When the evolution of strains decreases, the time step may increase consequently, and then limit the computation time.

Moreover, in the case of polymer materials, their cyclic behavior is difficult to grasp. They do not reach a stabilized state after few fatigue cycles like metals, but the cycle evolves slowly under the effect of creep at average stress, influenced by the strong coupling with the temperature when the frequency of solicitation is high. It has been shown in [9] that 200 cycles are not enough to reach the stabilized cycle for polypropylene under multiaxial fatigue. Therefore, the temporal domain becomes very large, which induces a very large computation time with a classical FEM. The time step should be chosen in order to simulate each cycle, and the simulation be performed until the last cycle.

Thus, this type of problems, especially when they involve a large number of cycles and a very large number of internal variables, is particularly CPU expensive. Model reduction can be an efficient way to obtain a tractable computational strategy. The most popular model reduction technique is the Proper Orthogonal Decomposition [10]. It consists in extracting a reduced number of functions able to represent the whole time evolution of the solution. The reduced model is then used to compute a similar model or a model with a larger time interval. Other model reduction strategies have been addressed as the LArge Time INcrement method [11–13] or the A Priori HyperReduction [14]. But, these methods are restricted to a space–time representation. A more general separated representation called Proper General Decomposition (PGD) was more recently employed by A. Ammar and F. Chinesta [15] for approximating the solutions of multidimensional partial differential equations. This method basically consists in constructing by successive enrichments an approximation of the solution in the form of a finite sum of N functional products involving d functions of each coordinate. These functions are not known a priori and are constructed on an iterative procedure based on a minimization problem [16–18]. Similar techniques have also been used in the stochastic framework [19] or in the multidimensional case [20–25]. The PGD avoids the use of an incremental strategy and can lead to impressive computing time savings, especially when the model involves a large number of degrees of freedom. For a complete and recent review of this method, the reader can refer to [22] and the references therein.

This paper focuses on the PGD solution of models described with a large number of differential equations coupled with a global and multiscale model through cyclic loading. In the framework of fatigue load, a multiscale technique can also be used. Ammar et al. [26] suggest reformulating the model by introducing different time coordinates allowing the expression of the solution from a multidimensional time approximation. The time scale considered in the illustrative examples is only due to the loading and leads to consider two time variables instead of one time variable. In our opinion, this technique is intractable for viscoelastic models where a large number of relaxation times are required.

The coupling between global and local equations and the issue related to the existence of different characteristic times of both the local and global problems have been investigated [21,27]. Three different ways are presented by Chinesta et al. [21] in the case of species kinetic local models. The first one consists in using a separated representation of the global problem solution, whereas the local problems are integrated in the whole time interval at each Gauss point. This strategy is similar to the finite-element one and involves, in the framework of the PGD, the use of the Singular Value Decomposition (SVD) in order to separate the solutions of the local problems. This step could be expensive and this strategy is not investigated in the paper. The second one consists in globalizing the solution of the local problems. All the problems are solved entirely with the PGD method. Compared to the first strategy, the application of the SVD is avoided. However, it is mentioned that if the number of species is high, the computation time becomes large, the space–time separated solver being applied to each species. The third strategy, which is investigated in detail in their paper [21], consists in adding an extra-coordinate that allows describing all the different species. The choice of the authors is well understandable as it leads to consider only one partial differential equation instead of the number of species. However their illustrative example concerns a global model partially coupled with a large number of kinetic species. It means that only the kinetic species influence the global model.

To our knowledge, the PGD has not been applied to viscoelasticity with a large number of internal variables and a large number of relaxation times, except in our previous work [28], where the application was restricted to creep test and only one internal variable with a same and regular time step for the displacement and the internal variable. Since in our model the global equations of balance and local evolution laws are completely coupled, we propose to apply the second strategy, which consists in only globalizing the solution of the local equations. The purpose is to discuss in detail the feasibility of this numerical strategy to predict viscoelastic behavior under creep and cyclic loading where different times are considered: one linked to mechanical loading and the others linked to the relaxation times induced by the consideration of internal variables. As the retained numerical strategy could be time consuming, we suggest here to investigate the possibility of considering different time discretizations: one for the displacement and another one for each internal variable.

In summary, the two major issues of the paper are: (i) to prove that the globalization strategy allows solving real viscoelastic models (50 internal variables) and (ii) to understand the link between relaxation times and time discretizations of the numerical method when the sought solution evolves at different time scales (the cycle time and the total time) to obtain a tractable computational strategy. The paper is organized as follows. The simplified (one-dimensional) viscoelastic model is described and the specificities of the PGD method are introduced in Section 2. Section 3 illustrates the globaliza-

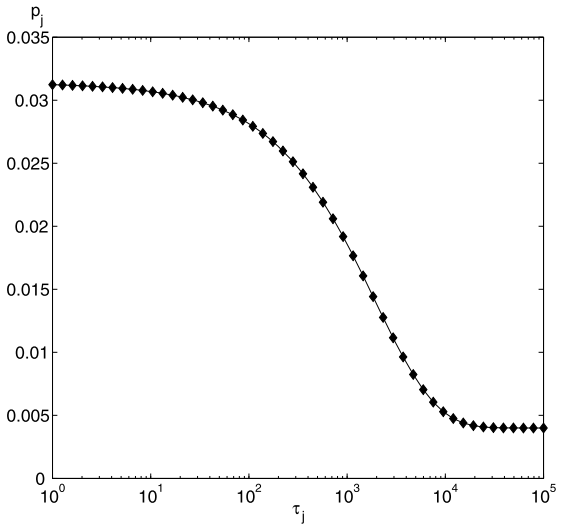

Fig. 1. Spectrum of weight distribution with respect to relaxation times.

tion strategy for polymers' viscoelasticity for two different loadings (creep and cyclic loading), which allows increasing the number of time scales. The results are discussed with respect to the number of internal variables (1 and 3) and different time discretizations related to the different time scales. Finally, a more realistic distribution requiring 50 internal variables is investigated, and precedes the conclusions in Section 4.

2. PGD method for the viscoelastic problem

2.1. Viscoelastic model

We are considering a one-dimensional mechanical equation with a particular viscoelastic behavior described by internal variables z_j. The generic form of the problem can be written as follows:

$$\frac{\partial \sigma}{\partial x} + f = 0 \tag{1}$$

$$\frac{\mathrm{d}z_j}{\mathrm{d}t} + \frac{1}{\tau_j}\left(z_j - z_j^{\infty}\right) = 0 \quad \forall 1 \le j \le m \tag{2}$$

where

$$\sigma = E_v \frac{\partial u}{\partial x} - \sum_{j=1}^{m} z_j \tag{3}$$

$$z_j^{\infty} = E_{rj}^{\infty} \frac{\partial u}{\partial x} \quad \forall 1 \le j \le m \tag{4}$$

Eq. (1) is the equilibrium equation where σ is the stress and f is the mechanical loading, which depends on space and time. Eq. (2) represents the kinetic of return to equilibrium and specifies the dependence of the relaxation times τ_j on the internal variables z_j. The equilibrium of process j is reached when the value of the corresponding internal variable z_j is equal to its value at the equilibrium, noted z_j^{∞}.

This internal equilibrium depends here linearly on the macroscopic variable $\frac{\partial u}{\partial x}$ such as formulated in Eq. (4), where the relaxed modulus at equilibrium E_{rj}^{∞} generated by the process j follows this equation:

$$E_{rj}^{\infty} = p_j E_r \quad \forall 1 \le j \le m \tag{5}$$

where E_r represents the relaxed modulus, E_v the vitreous modulus, and p_j the weights given by a distribution that some authors [7] link to jump atomic fluctuations in the polymer. Three parameters are required to define the spectrum of the distribution of the weights: the number of decades of the spectrum range, the number of processes and the largest relaxation time [29]. As an example, Fig. 1 depicts the spectrum of the distribution obtained with 50 times distributed along six decades of the time scale.

Remark. E_v is usually measured in a high-velocity experiment compared to the smallest relaxation time and E_r in a very slow experiment.

Eqs. (1) and (2) are assumed to be defined on the domain: $\Omega = \Omega_x \times \Omega_t$, where $\Omega_x = [0, L_x]$ and $\Omega_t = [0, L_t]$. The initial conditions are equal to zero for the displacement field and the internal variables and the boundary conditions are written as: $\underline{\underline{\sigma}}.\underline{n} = \underline{F}$ on $\partial\Omega_\sigma$ and $\underline{u} = \underline{0}$ on $\partial\Omega_u$.

This mechanical problem leads to strongly coupled linear equations between the displacement field (global model) and the internal variables (many local models). Indeed, the displacement influences the evolution of the internal variables (linearly in this simple viscoelastic model) and vice versa. Moreover, each internal variable has a specific time scale. Thus, a large number of relaxation times must be considered simultaneously.

Remark. The subscript j concerns the internal variables and it varies from 1 to m, where m is the number of internal variables. If we consider a problem with m internal variables, it means that Eq. (2) is reported m times. The specificity of each equation is related to the relaxation time of this internal variable.

2.2. Use of the PGD to solve the viscoelastic problem

To solve this problem, we first globalize the local models as suggested in [21] by considering the internal variables as functions of space and time. The solutions u and z of the coupled problem are sought under the form:

$$u(x,t) \approx \sum_{i=1}^{N} A_i(x) B_i(t) \tag{6}$$

$$z_j(x,t) \approx \sum_{i=1}^{N} C_{ji}(x) D_{ji}(t) \quad \forall 1 \le j \le m \tag{7}$$

At the enrichment step n of the PGD algorithm, the following approximations are already known:

$$u^n(x,t) = \sum_{i=1}^{n} A_i(x) B_i(t) \tag{8}$$

$$z_j^n(x,t) = \sum_{i=1}^{n} C_{ji}(x) D_{ji}(t) \quad \forall 1 \le j \le m \tag{9}$$

We wish to compute the next functional product $A_{n+1}(x)B_{n+1}(t)$ and $C_{j(n+1)}(x)D_{j(n+1)}(t)$ $\forall 1 \le j \le m$, which is denoted by $R(x)S(t)$ and $V_j(x)W_j(t)$ $\forall 1 \le j \le m$ for alleviating the notation.

As the displacement and the internal variables are strongly coupled, all the unknowns could be computed at each enrichment step as in our previous paper in the case of thermoviscoelasticity [30]. Let us here remark that the displacement field and the internal variables are completely interrelated, but each internal variable depends only on the value of the displacement. We here suggest to compute alternatively the functional products $R(x)S(t)$ and $V_j(x)W_j(t)$ $\forall 1 \le j \le m$. At each enrichment step, it leads to solve $m+1$ nonlinear problems as described below. For alleviating the notations without loss of generality, the equations are written by considering $f = f_x \cdot f_t$ and the following boundary conditions: $\sigma \cdot \vec{n} = F$ at $x = L_x$ where F depends only on time and $u = 0$ at $x = 0$.

1. Computing $R(x)S(t)$

The weak form related to Eq. (1) reads:

$$\int_\Omega (\operatorname{div}\sigma + f) u^* \,\mathrm{d}\Omega = 0 \tag{10}$$

for all test functions u^* selected in an appropriate functional space.

This equation is integrated by parts to take into account Neumann conditions:

$$\int_\Omega \frac{\partial u^*}{\partial x} \sigma \,\mathrm{d}x\,\mathrm{d}t = -\int_\Omega f u^* \,\mathrm{d}x\,\mathrm{d}t + \int_{\partial\Omega_\sigma} F(t) u^*(x = L_x, t)\,\mathrm{d}t \tag{11}$$

The stress σ being derived from Eq. (3) with the values z_j^n, and the trial and test functions being written as follows:

$$u(x,t) = \sum_{i=1}^{n} A_i(x) B_i(t) + R(x)S(t) \tag{12}$$

$$u^*(x,t) = R^*(x)S(t) + R(x)S^*(t) \tag{13}$$

Eq. (11) is a nonlinear problem with respect to $R(x)$ and $S(t)$ that must be solved by means of a suitable iteration scheme.

In this paper, an alternating-direction fixed-point algorithm is used. Each iteration consists of two steps that are repeated until convergence. The first step assumes $S(t)$ known from the previous iteration and computes an update for $R(x)$ with the following equation:

$$-E_v \int_{\Omega_x} \frac{\mathrm{d}R}{\mathrm{d}x}\left(\int_{\Omega_t} S^2 \mathrm{d}t\right)\frac{\mathrm{d}R^*}{\mathrm{d}x}\,\mathrm{d}x = R^*(L_x)\left(\int_{\Omega_t} FS\,\mathrm{d}t\right) + \left(\sum_{j=1}^{m}\sum_{i=1}^{n}\int_{\Omega_x}\frac{\mathrm{d}C_{ji}}{\mathrm{d}x}\left(\int_{\Omega_t} D_{ji}S\,\mathrm{d}t\right) + \int_{\Omega_x} f_x\left(\int_{\Omega_t} f_t S\,\mathrm{d}t\right)\right)R^*\,\mathrm{d}x$$
$$+ E_v \sum_{i=1}^{n}\int_{\Omega_x}\frac{\mathrm{d}A_i}{\mathrm{d}x}\left(\int_{\Omega_t} B_i S\,\mathrm{d}t\right)\frac{\mathrm{d}R^*}{\mathrm{d}x}\mathrm{d}x \tag{14}$$

Since all the functions involving time are already known, $R(x)$ can be solved by using any suitable discretization technique. From the just-updated $R(x)$, the second step updates $S(t)$ with the following equation:

$$-E_v \int_{\Omega_t} S\left(\int_{\Omega_x}\frac{\mathrm{d}R^2}{\mathrm{d}x}\,\mathrm{d}x\right)S^*\,\mathrm{d}t = R(L_x)\int_{\Omega_t} FS^*\mathrm{d}t + \left(\sum_{j=1}^{m}\sum_{i=1}^{n}\int_{\Omega_t} D_{ji}\left(\int_{\Omega_x}\frac{\mathrm{d}C_{ji}}{\mathrm{d}x}R\,\mathrm{d}x\right) + \int_{\Omega_t} f_t\left(\int_{\Omega_x} f_x R\,\mathrm{d}x\right)\right)S^*\mathrm{d}t$$
$$+ E_v \sum_{i=1}^{n}\int_{\Omega_t} B_i\left(\int_{\Omega_x}\frac{\mathrm{d}A_i}{\mathrm{d}x}\frac{\mathrm{d}R}{\mathrm{d}x}\,\mathrm{d}x\right)S^*\mathrm{d}t \tag{15}$$

Since all the functions involving space are already known, $S(t)$ can be solved by using any stabilized discretization technique.

This iterative procedure continues until reaching convergence. Then u^{n+1} is computed from the converged functions $R(x)$, $S(t)$.

Remark. At $n = 0$, $R(x)S(t)$ is solution to the related elastic problem (without internal variable).

2. Computing $V_j(x)W_j(t)$ $\forall 1 \le j \le m$

For each value of j, the weak form related to Eq. (2) reads:

$$\int_{\Omega}\left(\frac{\partial z_j}{\partial t} + \frac{1}{\tau_j}\left(z_j - z_j^{\infty}\right)\right)z_j^*\,\mathrm{d}\Omega = 0 \tag{16}$$

for all test functions z_j^* selected in an appropriate functional space.

The value of the internal variable at the equilibrium z_j^{∞} being derived from Eq. (4) with the value u^{n+1}, and the trial and test functions being written as follows:

$$z_j(x,t) = \sum_{i=1}^{n} C_{ji}(x)D_{ji}(t) + V_j(x)W_j(t) \tag{17}$$

$$z_j^*(x,t) = V_j^*(x)W_j(t) + V_j(x)W_j^*(t) \tag{18}$$

Eq. (16) is a nonlinear problem with respect to $V_j(x)$ and $W_j(t)$. An alternating-direction fixed-point algorithm is used as previously for the displacement. Each iteration consists of two steps that are repeated until convergence. The first step assumes $W_j(t)$ known from the previous iteration and computes an update for $V_j(x)$ with the following equation:

$$\left(\int_{\Omega_x} V_j\left(\int_{\Omega_t}\frac{\mathrm{d}W_j}{\mathrm{d}t}W_j\,\mathrm{d}t\right) + \frac{1}{\tau_j}\int_{\Omega_x} V_j\left(\int_{\Omega_t} W_j W_j\,\mathrm{d}t\right)\right)V_j^*\mathrm{d}x$$
$$= \frac{E_{rj}^{\infty}}{\tau_j}\sum_{i=1}^{n}\int_{\Omega_x}\frac{\mathrm{d}A_i}{\mathrm{d}x}\left(\int_{\Omega_t} B_i W_j\,\mathrm{d}t\right)V_j^*\,\mathrm{d}x - \sum_{i=1}^{n}\int_{\Omega_x} C_{ji}\left(\int_{\Omega_t}\frac{\mathrm{d}D_{ji}}{\mathrm{d}t}W_j\,\mathrm{d}t\right)V_j^*\,\mathrm{d}x - \frac{1}{\tau_j}\sum_{i=1}^{n}\int_{\Omega_x} C_{ji}\left(\int_{\Omega_t} D_{ji}W_j\,\mathrm{d}t\right)V_j^*\,\mathrm{d}x \tag{19}$$

Since all the functions involving time are already known, $V_j(x)$ can be solved by using any suitable discretization technique. From the just-updated $V_j(x)$, the second step updates $W_j(t)$ with the following equation:

$$\left(\int_{\Omega_t}\frac{\mathrm{d}W_j}{\mathrm{d}t}\left(\int_{\Omega_x}V_jV_j\,\mathrm{d}x\right)+\frac{1}{\tau_j}\int_{\Omega_t}W_j\left(\int_{\Omega_x}V_jV_j\,\mathrm{d}x\right)\right)W_j^*\mathrm{d}t$$
$$=\frac{E_{rj}^{\infty}}{\tau_j}\sum_{i=1}^{n}\int_{\Omega_t}B_i\left(\int_{\Omega_x}\frac{\mathrm{d}A_i}{\mathrm{d}x}V_j\,\mathrm{d}x\right)W_j^*\mathrm{d}t-\sum_{i=1}^{n}\int_{\Omega_t}\frac{\mathrm{d}D_{ji}}{\mathrm{d}t}\left(\int_{\Omega_x}C_{ji}V_j\,\mathrm{d}x\right)W_j^*\mathrm{d}t+\frac{1}{\tau_j}\sum_{i=1}^{n}\int_{\Omega_t}D_{ji}(t)\left(\int_{\Omega_x}C_{ji}V_j\,\mathrm{d}x\right)W_j^*\mathrm{d}t \tag{20}$$

Since all the functions involving space are already known, $W_j(t)$ can be solved by using any stabilized discretization technique.

This iterative procedure continues until reaching convergence. Then z^{n+1} is computed from the converged functions $V_j(x)$, $W_j(t)$.

Once the solutions u^{n+1} and all z_j^{n+1} are computed, the residuals are defined: Re_u, related to Eq. (1), and Re_{zj}, related to Eq. (2).

$$Re_u=\frac{(\int_{\Omega}(E_v\frac{\partial^2u}{\partial x^2}-\sum_{j=1}^{m}\frac{\partial z_j}{\partial x}+f)^2\mathrm{d}\Omega)^{\frac{1}{2}}}{\|u\|} \tag{21}$$

$$Re_{zj}=\frac{\max_j(\int_{\Omega}(\frac{\mathrm{d}z_j}{\mathrm{d}t}+\frac{1}{\tau_j}z_j-\frac{E_{rj}^{\infty}}{\tau_j}\frac{\partial u}{\partial x})^2\mathrm{d}\Omega)^{\frac{1}{2}}}{\|z_j\|} \tag{22}$$

where $\|\ \|$ stands for the L^2 norm.

The iterative procedure stops when $\max(Re_u, (Re_{zj}, j=1,..,n))$ is small enough. The solution of the coupled problem is then given by Eq. (8) for u and (9) for z_j.

A less expensive criterion is used in the following simulations and is based on the norm of the difference between the solution with $n+1$ modes and the solution with n modes with respect to the norm of the solution with n modes:

$$Re_u(n+1)=\frac{\|u_{n+1}-u_n\|}{\|u_n\|} \tag{23}$$

$$Re_{z_j}(n+1)=\max_j\left(\frac{\|z_j^{n+1}-z_j^n\|}{\|z_j^n\|}\right) \tag{24}$$

The error E with respect to the number of modes reads:

$$E(n+1)=\max\big(Re_u(n+1),Re_{z_j}(n+1)\big) \tag{25}$$

We can notice that the fields u and z_j are strongly coupled, i.e. with a strong reciprocal influence. If for example the residual corresponding to u is small enough, the corresponding field computation has to be carried on until the residual for all z_j is also small enough, the changes due to the computation for z_j being able to sensibly change the u values.

Before presenting the illustrative examples, the issue that deserves additional comments is the choice of the uncoupled strategy. In a previous paper [30], it has been shown that considering an uncoupled strategy for a linear problem leads to more modes than in the coupled strategy to accurately approximate the solution. It explains the number of modes obtained in the "Results" section. An interest of this strategy is the ability to use a parallel computation for the internal variables to decrease the computation time, but it is not the purpose of this paper. We here investigate the use of an adapted discretization to reduce the computation time. It is more general and will allow us to deal with nonlinear behaviors. In the case of nonlinearity, a coupled strategy will be more efficient.

3. Illustrative examples: a creep test and a cyclic loading

Since the PGD can be combined to a globalization concept to solve numerically local models, we investigate here the use of this strategy with viscoelastic models with very different relaxation times. For this purpose, we consider two different loadings: a creep loading and a cyclic loading, in order to study progressively the link between different characteristic times: the relaxation times, the loading time and the discretization time of the simulation. The aim is to answer the following questions:

- can we obtain an accurate solution with the PGD method?
- which time discretization should be chosen?
- is it possible to decrease the computation time by using different time steps for each internal variable?

For the subject related to the first question, different relaxation times are considered, leading to different responses of the polymer. The second question is related to the chosen PGD strategy. Let us recall that we consider the internal variables

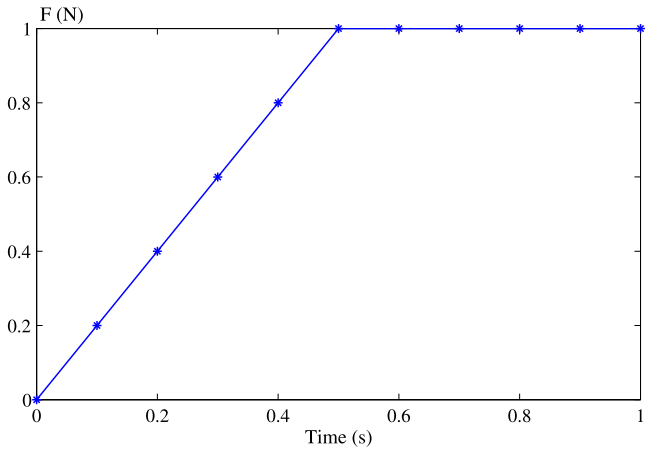

Fig. 2. Creep load at the extremity of the bar.

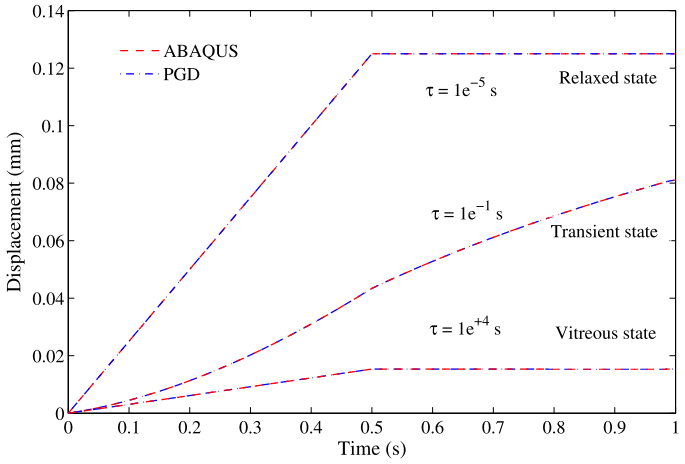

Fig. 3. Validation of the PGD versus *ABAQUS*^{TM}.

as global variables, the main default is that the computation time can become large because the space–time separated solver must be applied to each internal variable. To discuss this inconvenience, the simulations are discussed with respect to different time steps.

3.1. Creep test

The simulation test is a 5-mm-long one-dimensional bar clamped at $x = 0$ and subject at $x = 5$ to a time load $F(t)$ depicted in Fig. 2. The time domain L_t equals 1 s. The considered polymer is polypropylene and has the following properties: $E_r = 1000$ MPa, $E_v = 1140$ MPa. For the creep simulations, only one internal variable is considered to describe the transient behavior of the polymer, which leads to $p_1 = 1$ in Eq. (5).

The results obtained with the PGD are first compared for different relaxation times with the Standard *Abaqus*^{TM} Finite Element code with a same time step Δt equal to $1e^{-2}$ s and a same spatial step Δx equal to $5e^{-1}$ mm. A good agreement is observed as shown in Fig. 3, since the relative error is less than 3%. We can notice that the considered values of the relaxation time allow describing the different behaviors that can be observed for a polymer: the vitreous state, the transient state, and the relaxed state. These different behaviors are related to the evolution of the internal variable with respect to time (Eq. (2)).

Since the implementation of the globalization strategy is validated with a same time step to describe all the variables (internal variable and displacement), we next investigate the use of different time steps for different values of the relaxation time by keeping constant the characteristic time of the load. Relaxation times graduated on nine decades and two different time discretizations (Δt equals 0.1 s and Δt equals $1.25e^{-4}$ s) are considered. We can recall that the characteristic time of the load is 0.5 s for the transient part and 0.5 s for the constant part. The obtained results are depicted in Fig. 4. For all relaxation times larger than 10^2 (respectively smaller than 10^{-3}), the displacement corresponds to the vitreous state (the relaxed state). Between these relaxation-time values, the transient state operates. If the results are compared with respect

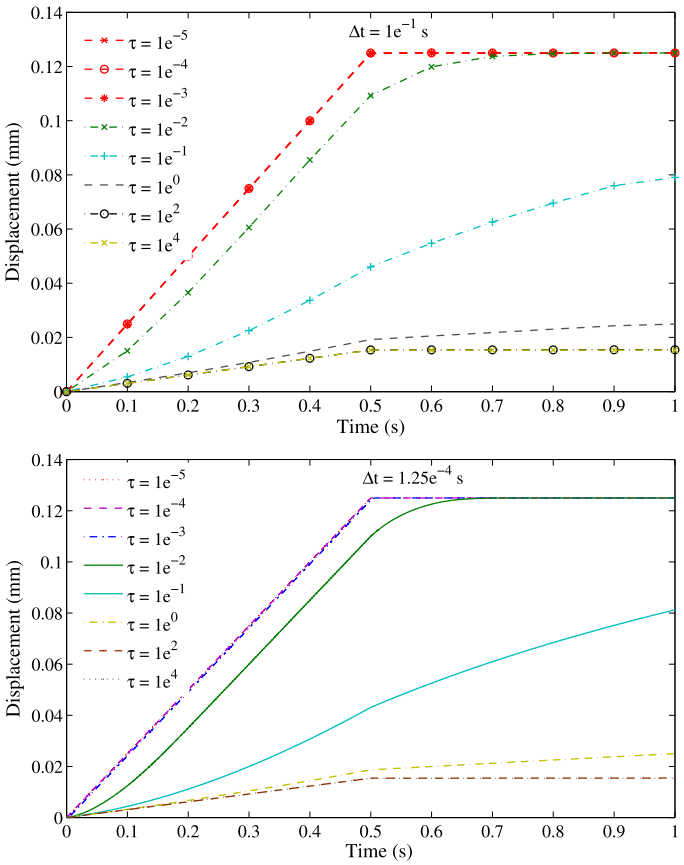

Fig. 4. (Color online.) Displacement with respect to time for different relaxation times: coarse (up) and fine (down) scales.

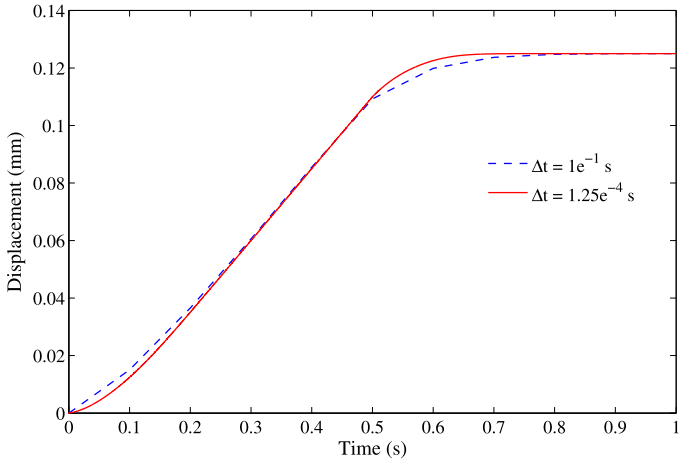

Fig. 5. Transient solutions obtained for $\tau = 10^{-2}$ s with respect to the time step.

to discretization time, differences are obtained only for the transient state as detailed in Fig. 5 for a relaxation time equal to 10^{-2}. Indeed, in the case of the vitreous state (very large relaxation time) and the relaxed state (very small relaxation time), the evolution of u depends mainly on the evolution of the creep load. Therefore, a time discretization of 0.1 s is efficient to describe the response to this particular load. Table 1 shows the number of PGD modes with respect to the relaxation time, and time discretization for an identical value of the stopping criteria of 10^{-3}. We observe that the description of the transient state necessitates a higher number of modes than the other states. It seems that the number of modes is more sensitive to the relaxation time compared to the time step.

Table 1
Number of PGD modes with respect to the relaxation time (τ) and the time steps ($\Delta t_1 = 1.25\text{e}^{-4}$ s and $\Delta t_2 = 1\text{e}^{-1}$ s).

τ (s)	1e^{-5}	1e^{-4}	1e^{-3}	1e^{-2}	1e^{-1}	1e^{0}	1e^{2}	1e^{4}
Δt_1	3	3	3	15	16	8	5	4
Δt_2	3	3	3	15	17	8	5	4

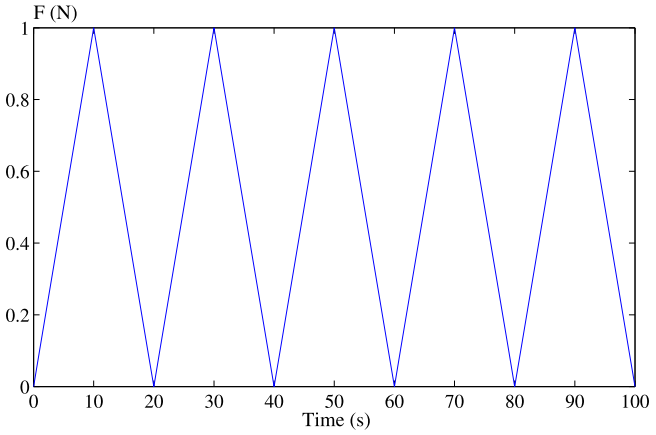

Fig. 6. The first five cycles of cyclic loading.

To illustrate the computational efficiency of the PGD method, the simulation which corresponds to $\tau = 0.1$ s and $\Delta t = 0.1$ s is performed with the Finite-Element Method. The computation time is reduced by a factor around 31 with the PGD method (more precisely 4 s instead of 125 s with the FEM).

In summary, the PGD allows predicting the viscoelastic behavior of a polymer under creep test and reducing computation time with respect to FEM. When the relaxation time of an internal variable is small or large enough (relaxed or vitreous states), a coarse scale related to the loading one can accurately predict the behavior of the polymer and a minimum number of modes is required. However, a fine scale (less than the creep load) is needed to describe the transient states and a large number of modes is required (17 instead of 4 for the other states of the polymer). Time discretization depends on the physical time (the relaxation time) and the characteristic time of the load, but this link is not trivial in this particular case. In the extreme cases (vitreous and relaxed states), the characteristic time of the load drives time discretization. Intermediate case generates a transient response, which is the consequence of the relaxation times, and thus time discretization should be adapted. But if there are many relaxation times, both previous situations (extreme and intermediate) can appear and then the previous conclusions cannot be extended.

3.2. Cyclic loading

In order to complete these results, a cyclic loading and different numbers of relaxation times are considered. The aim is to understand well the relationships between the different characteristic time scales in order to reduce computation time by adapting time discretizations. Firstly, a study with only one internal variable is investigated as in the case of the creep test to discuss the effect of the cycle time on time discretization. Different relaxation times are then investigated in order to discuss the extension of these results to a realistic distribution of 50 relaxation times.

3.2.1. One internal variable: influence of the relaxation time with respect to the time step

Let us replace the creep load $F(t)$ by a cyclic loading as depicted in Fig. 6. The time domain L_t equals 1000 s and leads to consider 50 cycles (20 s/cycle). The length of the bar and the material properties remain the same as in the case of creep test.

To discuss the efficiency of the PGD method to simulate the behavior of the polymer under cyclic loading, three different relaxation times are investigated:

- smaller than the cycle time: 1 s;
- in the same order of magnitude as the cycle time: 10 s;
- larger than the cycle time: 1000 s.

Fig. 7 depicts the solution of the displacement with respect to time for these three relaxation times. Different behaviors are generated with respect to relaxation times. When the relaxation time is smaller than the cycle time, the stabilized cycle is quickly reached (analogously to the relaxed state in the case of the creep test) and the internal variable influences

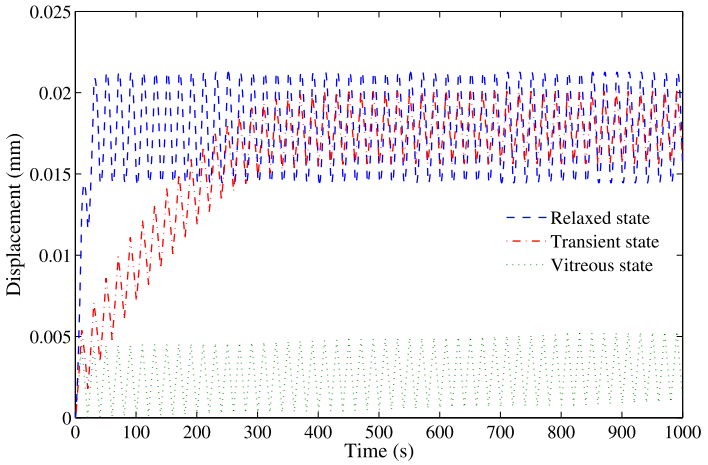

Fig. 7. (Color online.) Displacement under cyclic loading with respect to time for different relaxation times ($\tau = 1$ s, $\tau = 10$ s and $\tau = 1000$ s).

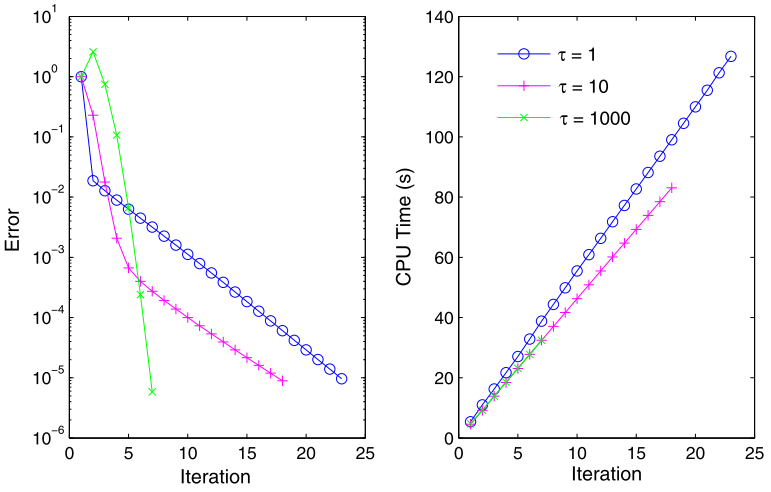

Fig. 8. (Color online.) Convergence and CPU time with respect to the number of modes.

mainly the first cycles. When the relaxation time is in the same order of magnitude as the cycle time (transient state), the displacement goes toward the stabilized cycle at the end of the simulation. When the relaxation time is larger than the cycle time, the stabilized cycle is not reached at the end of the simulation, the internal variable evolving very slowly on this time scale. More than 50 cycles are required to reach this stabilized cycle.

Fig. 8 shows the evolution of the numerical error (Eq. (25)) and the total computing time on a laptop with respect to the number of modes for these three relaxation times. For a level error equal to 10^{-5}, the number of PGD modes is the following: 23 for $\tau = 1$ s, 18 for $\tau = 10$ s and 7 for $\tau = 1000$ s.

In Figs. 9, 10 and 11, we illustrate the normalized functions $B_i(t)$ and $D_i(t)$. For the normalized functions $B_i(t)$, which correspond to the displacement, we observe that the first mode is the same for all values of τ and represents the elastic mode, due to the use of the uncoupled strategy. After that, the modes progressively take into account the coupling between the displacement and the internal variable. They differ according to the value of τ, the progressive influence of the viscosity implying an increasing phase delay. For $\tau = 1$ s, more modes are needed to reach the permanent regime. As in this case there is no spatial dependency for z and as τ is smaller than the cycle time, the evolution of z is close to that of z^{∞} (Eq. (4)), and we obtain the same time normalized functions for u and z except for the first mode. For $\tau = 10$ s, the time evolutions of z and u are different, leading to different modes. The phase delay increases more quickly, the viscosity is captured by less modes. For $\tau = 1000$ s, the evolution of z is close to 0 as the total time is too small.

In summary, the shape of the time modes are linked to the choice of the uncoupled strategy, taking into account mode per mode the coupling effect and then the relaxation phenomenon.

As the considered time domain must be larger in the case of the largest relaxation time, a question is: can we limit the computation time by considering an adapted time step?

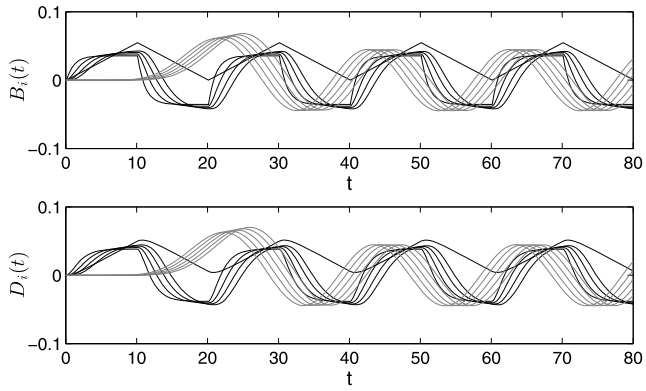

Fig. 9. Normalized time functions for $i = 1, \ldots, 5$ (black) and $i = 19, \ldots, 23$ (grey) in the PGD solution for $\tau = 1$ s.

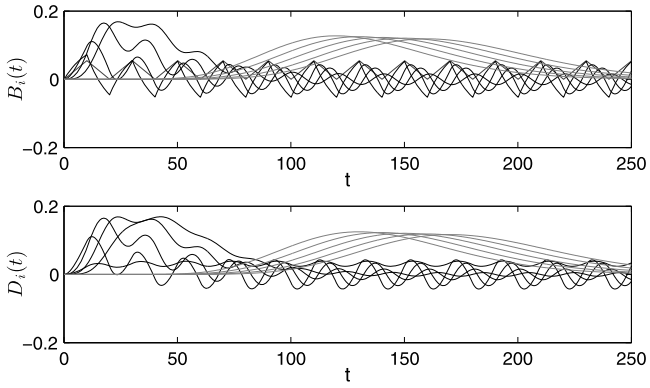

Fig. 10. Normalized time functions for $i = 1, \ldots, 5$ (black) and $i = 14, \ldots, 18$ (grey) in the PGD solution for $\tau = 10$ s.

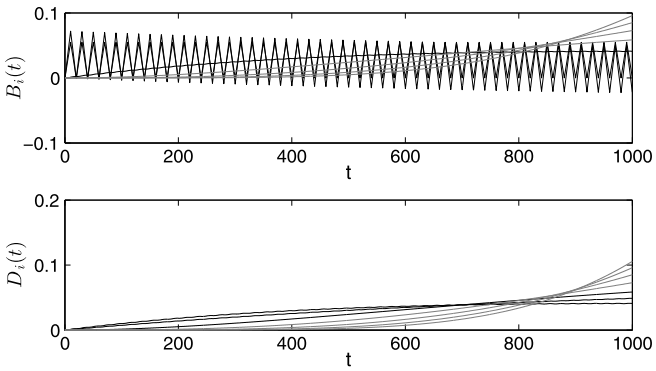

Fig. 11. Normalized time functions for $i = 1, \ldots, 3$ (black) and $i = 4, \ldots, 7$ (grey) in the PGD solution for $\tau = 1000$ s.

For this purpose, we firstly consider a relaxation time equal to 1 s. The resulting displacement is depicted in Fig. 12 with respect to time for the three different time steps ($\Delta t = \frac{L_t}{N_t}$). These time steps are related to the cycle time as follows: $N_t = [8001, 6001, 2001, 501, 101]$ represents respectively $[161, 121, 41, 11, 3]$ points per cycle.

The general shape of the displacement is similar for all time steps, especially when the number of time points (N_t) is larger than 501 (11 points per cycle). But if we zoom in, we can observe a significant phase shift and magnitude between the fine and coarse scales. To establish the relationship between the time step and the relaxation time, the same simulations are performed by considering the other relaxation times, and the results are discussed as follows. We denote by the subscript 161 the value of the field with a time step that leads to 161 points per cycle. This case corresponds to the reference one and represents the finest time step that is considered.

To illustrate the convergence of the PGD solution to the reference solution, we define the following relative error between the reference solution for the displacement $u_{\text{ref}}(x, t)$ and a numerical PGD solution with N terms:

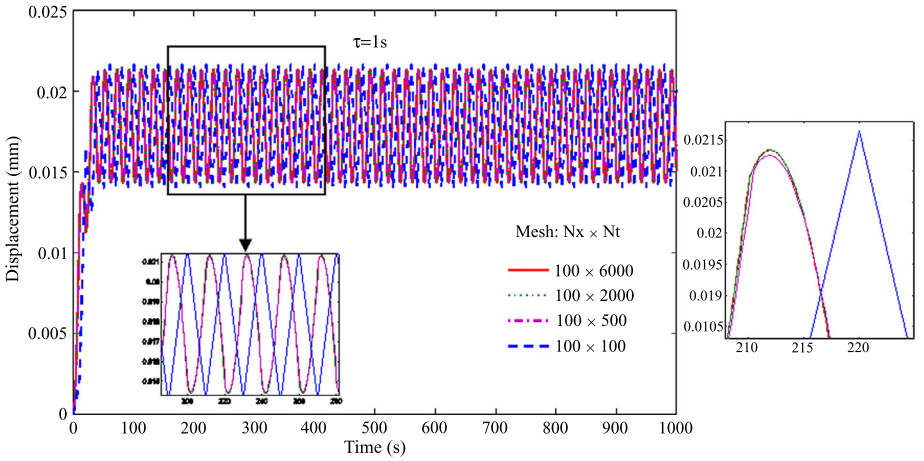

Fig. 12. (Color online.) Displacement under cyclic loading with respect to time for different time steps.

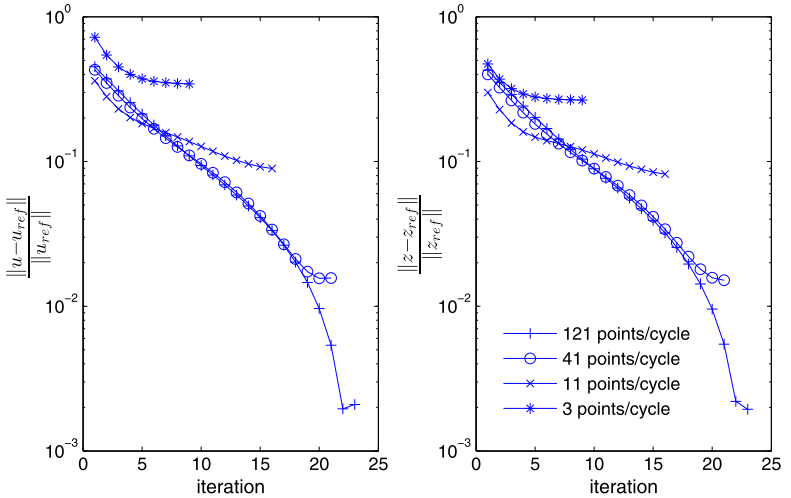

Fig. 13. Relative PGD error $Er(u^N)$ and $Er(z^N)$ as a function of the number of modes for different time steps.

$$Er\left(u^N\right) = \frac{\int_\Omega (u^N - u_{\text{ref}})^2 \mathrm{d}x\,\mathrm{d}t}{\int_\Omega u_{\text{ref}}^2 \mathrm{d}x\,\mathrm{d}t} \tag{26}$$

We use the same definition for the internal variable z^N with respect to z_{ref}. In Fig. 13, we illustrate the global convergence towards the reference solution for the different time steps. The relative error decreases with the number of modes, until the last mode, for which we see that a threshold has been reached. This means that the optimal number of modes has been computed, which validates the value of the stopping criterion used for the PGD algorithm (here 10^{-5}). To discuss in detail the sensitivity and the accuracy of the results with respect to the time steps, we choose to represent the relative difference between the field and the reference field. All these fields are evaluated on the same spatial and time point, which corresponds to the last cycle and the point at the extremity. The results are depicted in Fig. 14 for the displacement field and in Fig. 15 for the internal variable for different relaxation times. Let us consider the displacement field in Fig. 14. When the relaxation time is less than the cycle time (left-hand curves on the left), this magnitude will remain constant approximately when the time discretization is larger than 121 points/cycle, and when the relaxation time is larger than the cycle time (right-hand curves), this magnitude will remain constant approximately after 21 points/cycle.

With a large relaxation time, the number of points per cycle does not need to be large to have an accurate magnitude of the displacement field. Consequently, a fine discretization is not required and then a higher number of cycles can be simulated. The same tendency is obtained for the magnitude of the internal variable, as shown in Fig. 15. Let us take a look at the phase shift with respect to the number of points per cycle (Fig. 16). The value of the phase shift drops down to zero after around 61 points/cycle when the relaxation time is more than the cycle time, which is unachieved when the relaxation time is less than the cycle time.

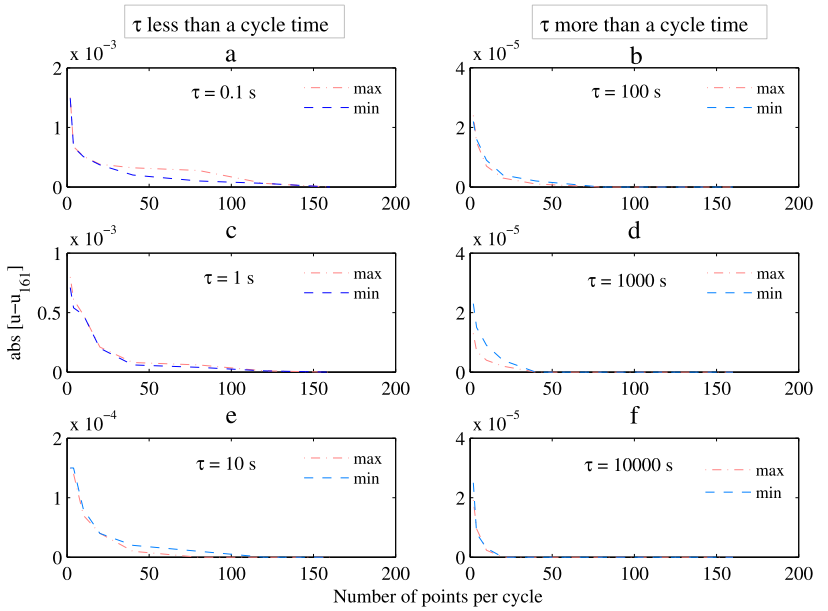

Fig. 14. Influence of the time step on the accuracy of the magnitude of the displacement field for different values of τ.

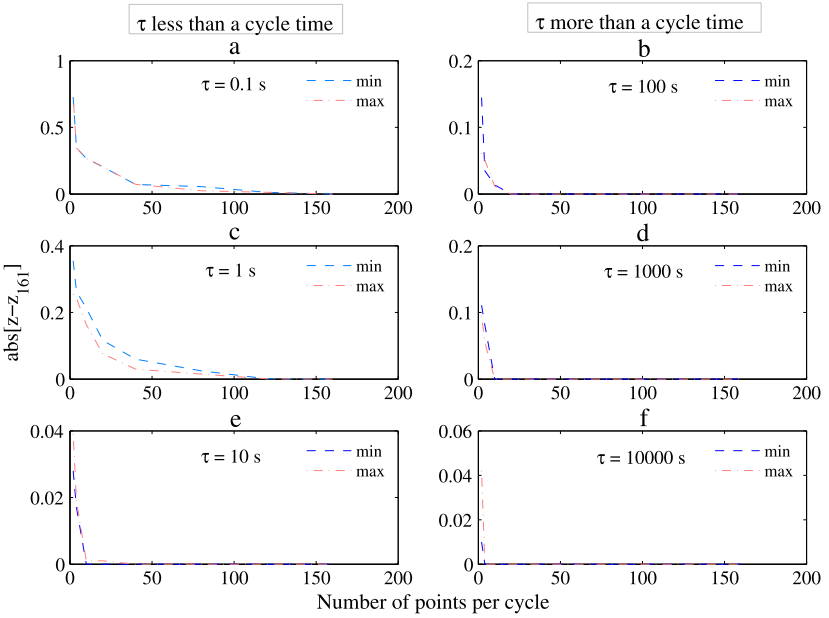

Fig. 15. Influence of the time step on the accuracy of the magnitude of the internal variable for different values of τ.

From these simulations, we can conclude that when the relaxation time is larger than the cycle time, a coarse scale is adequate to simulate the behavior of the polymer. Otherwise, a fine scale is needed when the relaxation time is smaller than the cycle time.

3.2.2. Three internal variables with same time basis and different relaxation times

As the viscoelastic behavior is usually described by a large number of internal variables, we next analyze whether the above conclusions are still valid in the case of three internal variables. For this purpose, the triplets of relaxation times are as follows:

- smaller than the cycle time [0.1, 1, 10] s,
- in the same order as the cycle time [1, 10, 100] s,

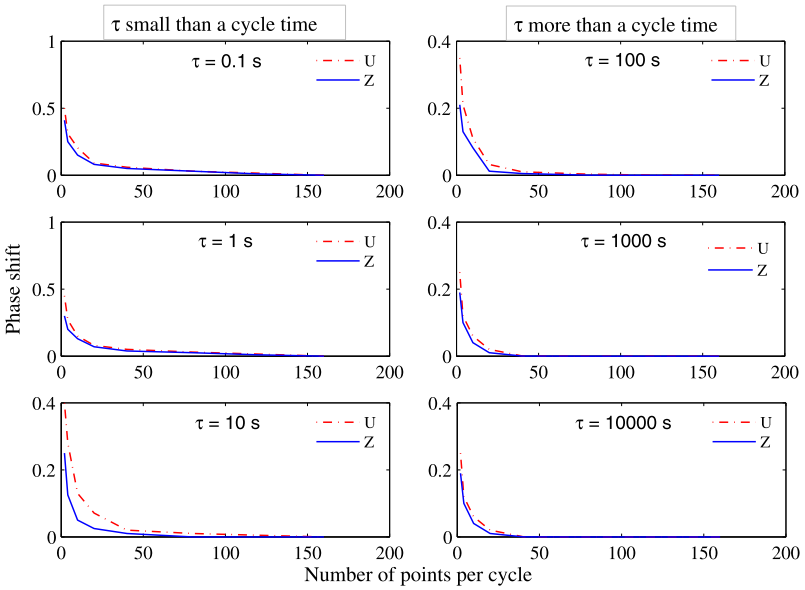

Fig. 16. Influence of the time step on the phase shift for different values of τ.

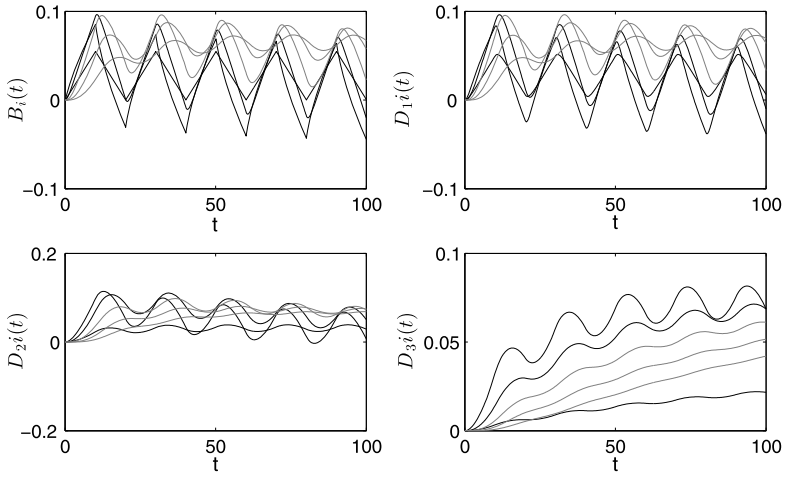

Fig. 17. Normalized time functions for $i = 1, \ldots, 6$ in the PGD solution for the triplet $\tau = [1, 10, 100]$ s.

– larger than the cycle time [100, 1000, 10000] s and for each triplet of relaxation times, the time step will take the following set of values: [3, 11, 21, 81, 121, and 161] points/cycle.

As an example, we illustrate in Fig. 17 the normalized functions $B_i(t)$, $D_{1i}(t)$, $D_{2i}(t)$ and $D_{3i}(t)$ for $i = 1, \ldots, 6$ in the case where the relaxation times are [1, 10, 100] s, with 161 points per cycle. The first mode for u is the elastic one. The second mode is only affected by the relaxation time $\tau = 1$ s, and the following modes gradually take into account the influence of the larger relaxation times. The same behavior appears for the modes of z.

To analyze the accuracy of the solution with respect to the time step, the magnitude of the relative displacement field with respect to the number of points per cycle is depicted in Fig. 18 and the phase shift is depicted in Fig. 19. The same conclusion as in the case of one internal variable is available. When the relaxation time is larger than the cycle time, a coarse scale can be used.

We can notice that the solution for each of the above cases is obtained after 8 modes (which smaller than a cycle time), 14 modes (which is in the same order of magnitude as a cycle time) and 10 modes (which is larger than a cycle time); convergence is reached respectively after 121 points/cycle, 81 points/cycle, and 21 points/cycle.

Thus, we can generalize the relationships between different time scales and the benefits will then be used in the case of many internal variables with adequate time basis.

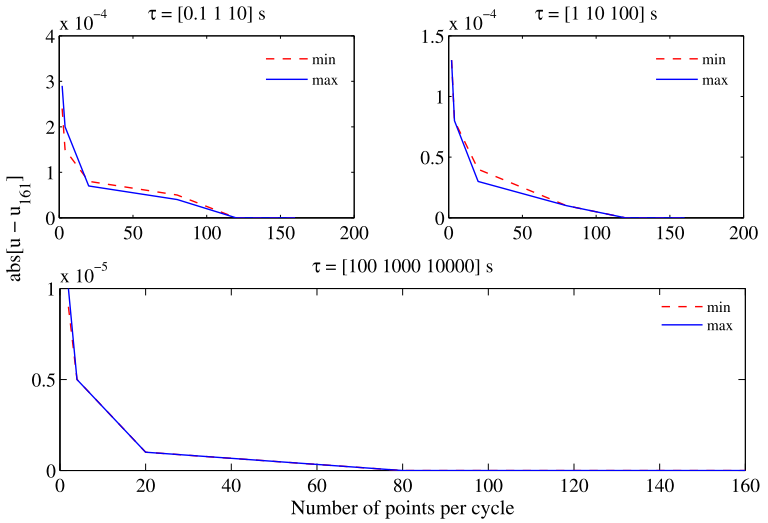

Fig. 18. (Color online.) Influence of the time step on the accuracy of the magnitude of the displacement for different values of the relaxation times.

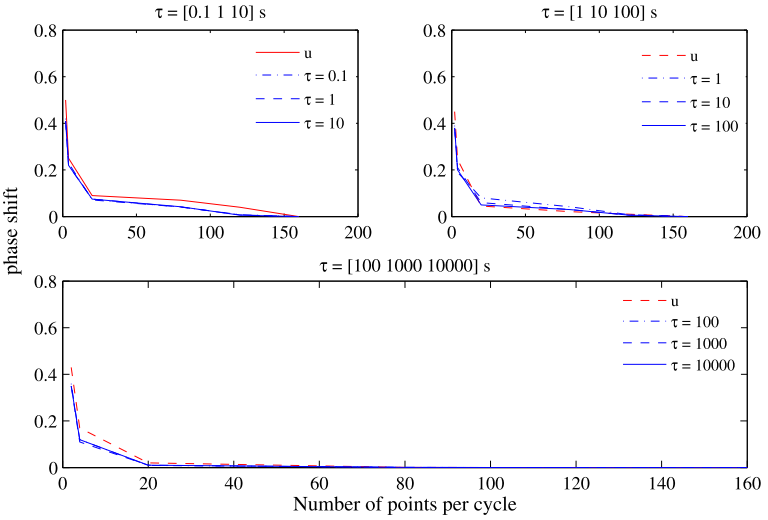

Fig. 19. (Color online.) Influence of the time step and the relaxation times on the accuracy of the phase shift.

Table 2
Gain ratio of computation time with respect to the finer scale (161 points/cycle).

Number of points/cycle	3	11	21	81
$\tau = [0.1, 1, 10]$ s	11.2	9.3	6.2	3.2
$\tau = [1, 10, 100]$ s	9.5	8.1	5.2	2.5
$\tau = [100, 1000, 10000]$ s	10.3	8.5	5.7	2.9

Regarding computation time, Table 2 illustrates the gain ratio of each time scale with respect to the finer scale (which corresponds to the solution 161 points/cycle). For example, in the case of relaxation times larger than the cycle time where the convergence is reached after 21 points per cycle, the gain ratio is equal to 5.7.

3.2.3. Three internal variables with different time basis

The behavior of the polymer is well described using three internal variables with the same time basis for all the variables. But this leads in some cases to a large computation time even if the time basis can be coarser if the relaxation times are larger than the cycle time, so in this section we will try to decrease it by finding an adequate time basis for each internal variable.

Let us begin with the case of $\tau = [0.1, 1, 10]$ s, where the relaxation times are smaller than the cycle time and consider different time steps for each internal variable.

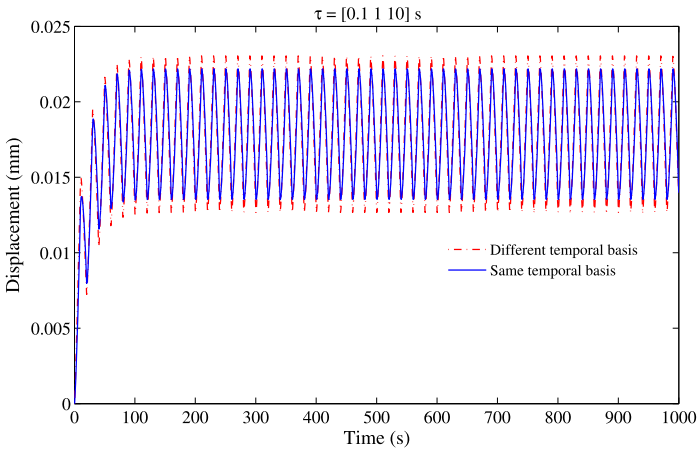

Fig. 20. (Color online.) Comparison between the displacement fields for different time discretizations: same basis ($n_{t_z} = 6001$) and different basis ($n_{t_z} = [6001, 1001, 101]$ respectively for $\tau = [0.1, 1, 10]$ s) in the case of three internal variables.

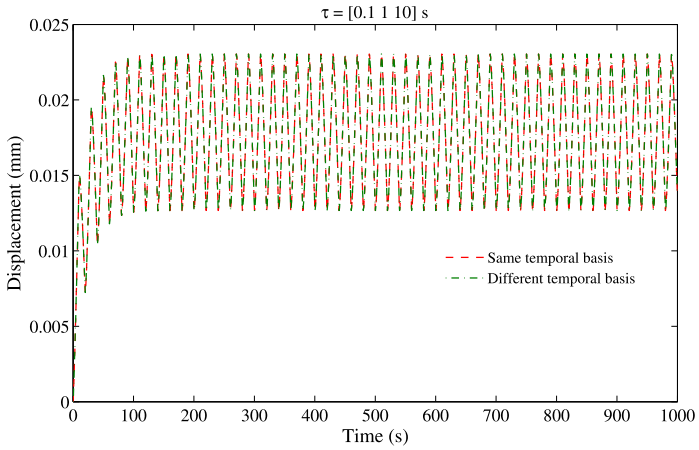

Fig. 21. (Color online.) Comparison between the displacement fields for different time discretizations: same basis ($n_{t_z} = 6000$) and different bases ($n_{t_z} = [6001, 4001, 1001]$ respectively for $\tau = [0.1, 1, 10]$ s) in the case of three internal variables.

Remark. Let us define n_{t_z} and n_{t_u} – which will be used later in the following simulations – as the number of time discretization of the internal variable and the displacement, respectively.

A comparison between the displacement fields obtained with three internal variables with same and different time bases is depicted in Fig. 20. A major difference is noticed for the magnitude. It means that the time bases are not suitable for some internal variables. If we use the results obtained with one internal variable depicted in Fig. 15, more than 81 points per cycle (4001 points) had to be used for relaxation times equal to 0.1 s and 1 s instead of 21 points per cycle (1001 points) for a relaxation time equal to 10 s. The numbers of time points are then inadequate for these two relaxation times. The previously prescribed time steps are then considered and the results are depicted in Fig. 21. An accurate displacement is obtained as expected.

Concerning the computation time, we observe that the gain ratio increases when the bases are different. A gain ratio of about 3 is reached with this different basis by comparison with the same basis (161 points per cycle). The number of modes remains almost constant: 8 modes (same basis) instead of 7 modes (different basis).

Let us consider another case with relaxation times equal to $\tau = [1, 10, 100]$ s (same order of magnitude as the cycle time). The considered time bases are respectively $[81, 41, 11]$ points per cycle for $\tau = [1, 10, 100]$ s. These bases are efficient to obtain an accurate solution as depicted in Fig. 22 and cannot be more decreased as shown in Fig. 14.

The computation time here decreases with a gain ratio equal to 5 by comparison with the simulation of a same basis (161 points/cycle) for all the internal variables. The number of modes does not evolve significantly: 12 modes (different basis) instead of 14 modes (same basis). The gain ratio is larger than in the previous case ($\tau = 0.1$ s, $\tau = 1$ s and $\tau = 10$ s), despite a large number of modes, the chosen basis being more coarse.

Let us finally consider that all the relaxation times are greater than the cycle time: $\tau = [100, 1000, 10000]$ s. The previous study with one internal variable ensures that a coarse time scale is sufficient to simulate the behavior. As suggested in

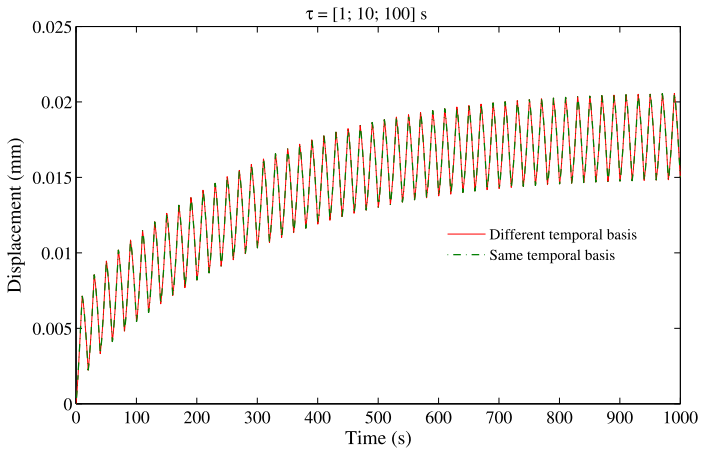

Fig. 22. (Color online.) Comparison between the displacement fields for different time discretizations: same basis ($n_{t_z} = 6001$) and different bases ($n_{t_z} = [4001, 2001, 501]$ respectively for $\tau = [1, 10, 100]$ s) in the case of three internal variables.

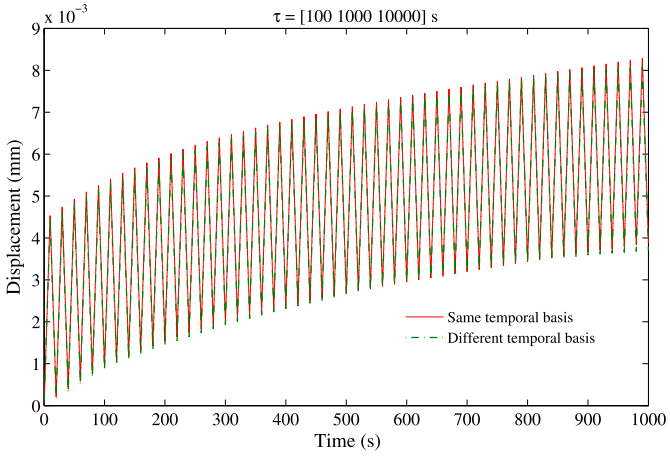

Fig. 23. (Color online.) Comparison between the displacement fields for different time discretizations: same basis ($n_{t_z} = 101$) and different bases ($n_{t_z} = [11, 5, 3]$ respectively for $\tau = [100, 1000, 10000]$ s) in the case of three internal variables.

Fig. 14, a simulation with respectively $[11, 5, 3]$ points for $\tau = [100, 1000, 10000]$ s is performed and leads to an accurate result as depicted in Fig. 23. The gain ratio of the computation time equals 8 and the number of modes is 3 instead of 5 in the case of the same basis for all the internal variables.

3.2.4. Three internal variables with a space dependence

In all the previous simulations, as the force is concentrated at an extremity of the bar, the spatial dependence is quite trivial and requires only one spatial mode that remains constant along the bar. Let us consider again the case with three internal variables and relaxation times $\tau = [1, 10, 100]$ s (same order of magnitude as the cycle time). We investigate here another loading which induces spatial gradient to conclude on the robustness of such globalization and adapted time discretizations when space localization occurs. In these simulations, a distributed force along the bar $f(x, t)$ is added to the previous one. The force $f(x, t)$ is the following:

$$f(x, t) = F(t) \times 10 \sin(5\pi x/2), \tag{27}$$

where $F(t)$ is defined as previously (Fig. 6).

The displacement here evolves with respect to space and time, as depicted in Fig. 24. Two spatial modes are needed to describe this spatial evolution. Fig. 25 illustrates the obtained displacement at three different spatial points ($x = 0$, $x = 2.5$ and $x = 5$) for three different time discretizations: same basis ($n_{t_z} = 6001$), and two different bases, (*i*) $n_{t_z} = [4001, 2001, 501]$ respectively for $\tau = [1, 10, 100]$ s, (*ii*) $n_{t_z} = [501, 201, 101]$ respectively for $\tau = [1, 10, 100]$ s. Let us note that space discretization remains constant for all the simulations, the objective being to ensure that adapted time discretizations remain an efficient way when spatial localization occurs.

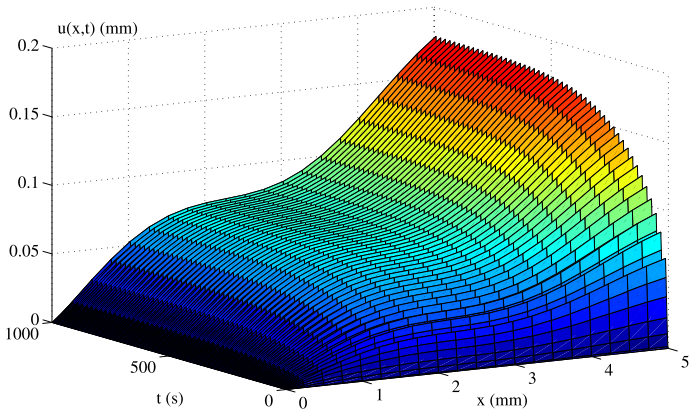

Fig. 24. (Color online.) Displacement in the case of the spatial dependence.

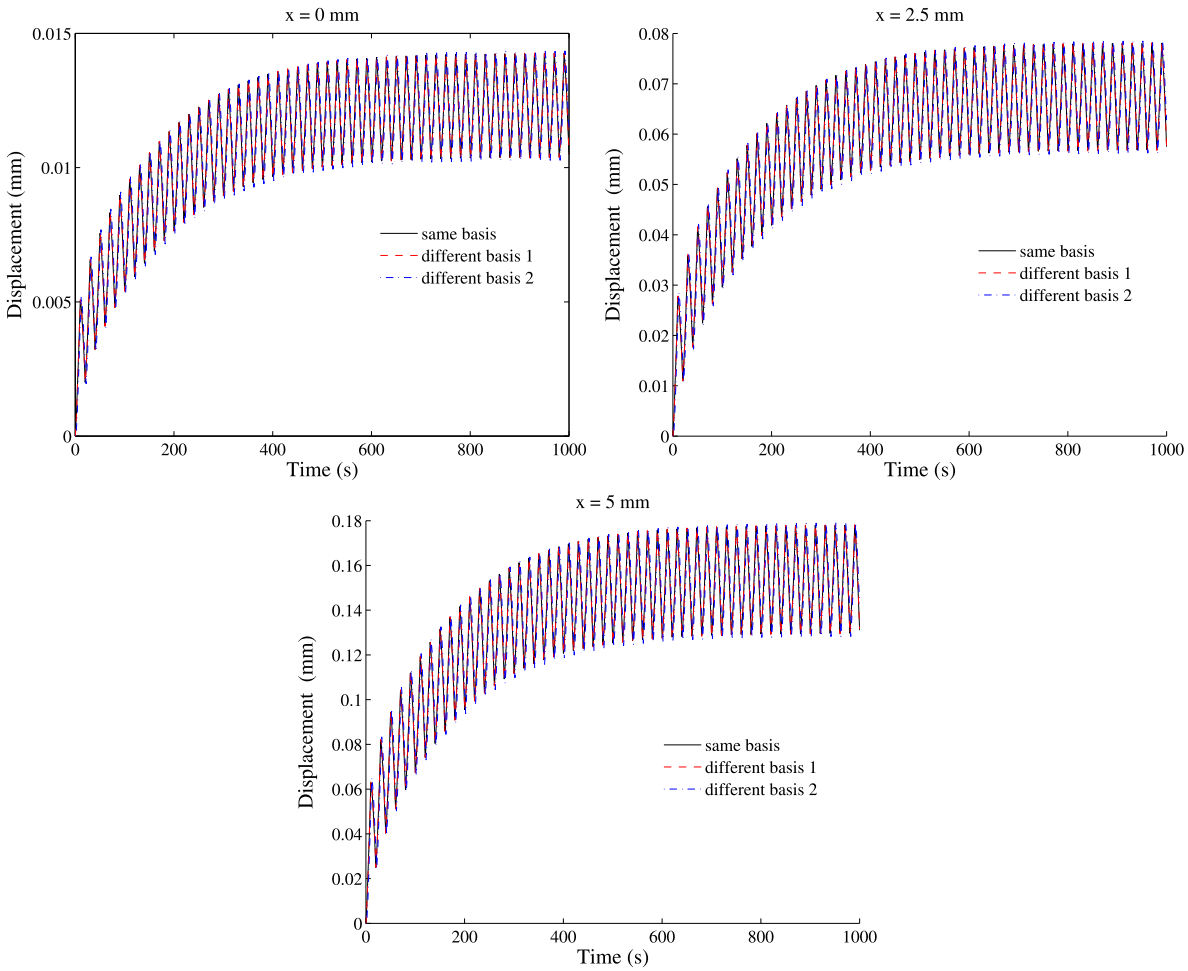

Fig. 25. (Color online.) Displacement with respect to time at different spatial points for three different bases.

We obtain the same results as previously (without spatial dependence). The displacement is accurate along x and t for time basis 1, time basis 2 being too coarse, as illustrated more precisely in Fig. 26. Computation time is reduced by a factor 4.25 with respect to the simulation with a same time step for all the variables.

In summary, the globalization strategy is an efficient way to predict models with a large number of internal variables, in the framework of the PGD. In the case where spatial gradients are observed, adapted time discretizations are always an efficient way to decrease computation time without loss of accuracy.

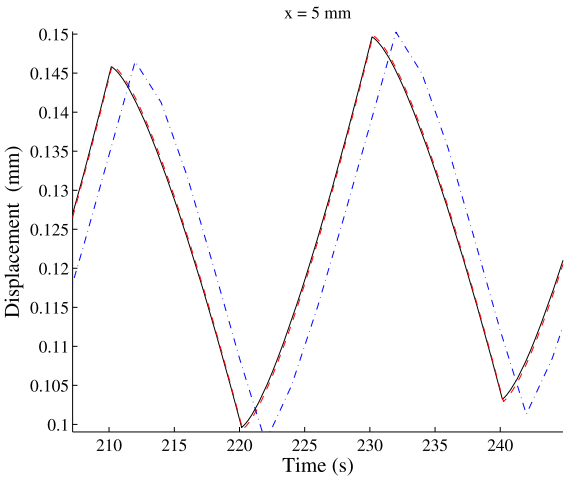

Fig. 26. (Color online.) Zoom in on the displacement at $x = 5$ mm.

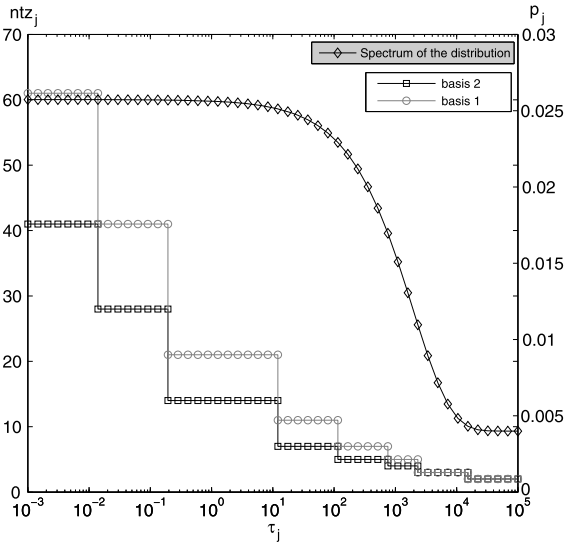

Fig. 27. Spectrum of the distribution of the weights with respect to the relaxation times and the number of time points with respect to the relaxation times for the two different time bases.

3.2.5. A realistic distribution of 50 internal variables

Let us now consider a realistic distribution of the relaxation times spread over 8 decades (10^{-3}–10^{5}). Fifty relaxation times are considered to correctly discretize this continuous distribution, as suggested by Cunat [6], leading to simulate a viscoelastic model with 50 internal variables. The distribution of weights p_j (Eq. (5)) with respect to τ_j is depicted in Fig. 27. In this case, the restricted simulations with a time load at the extremity of the bar are performed, and the results are discussed with respect to the time discretizations. Three different time discretizations are investigated: same basis ($n_{t_z} = 6001$) and two different bases (Fig. 27).

The obtained displacement at the end of the bar is plotted with respect to time in Fig. 28 for these three basis. The first adapted time basis allows us to have a good accuracy (magnitude and phase shift), as shown in Fig. 28. These results are not surprising and allow us to generalize those obtained with three internal variables. From a computational point of view, the first adapted basis allows a gain ratio of 4.8 with respect to the same basis.

Remark. τ_j is the relaxation time specific to the internal variable j and nt_{z_j} is the time basis for each internal variable.

In summary, the PGD method with globalization of the local models is efficient to predict polymers fatigue when the viscoelastic model is described with a large number of internal variables. The computation time can be significantly reduced by considering adapted time discretizations. To adapt these discretizations, without loss of accuracy, it is mandatory to take into account the relaxation times versus the cycle time.

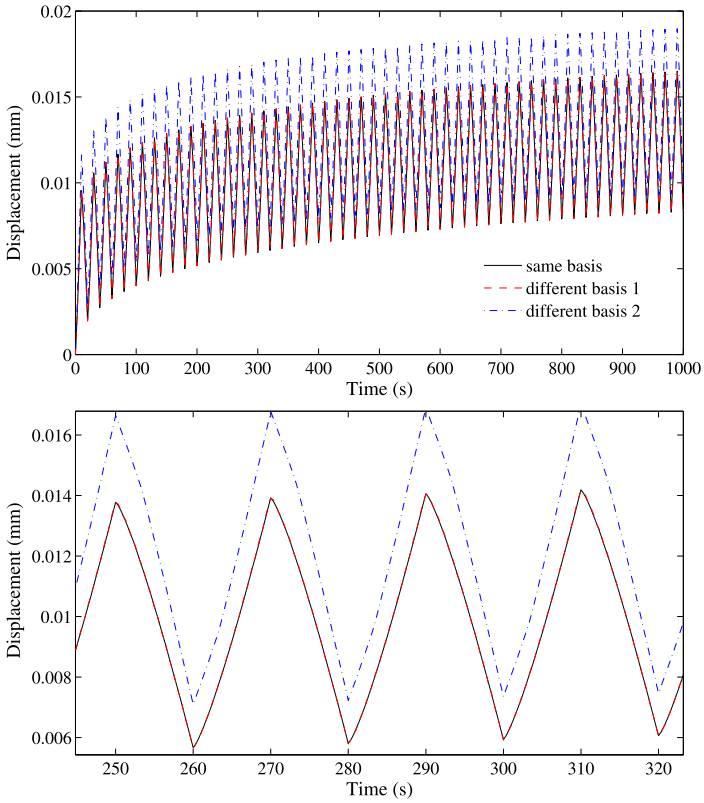

Fig. 28. (Color online.) Displacement with respect to time for the three different time discretizations (same basis, different basis 1, different basis 2) in the case of 50 internal variables (top) and zoom-in (bottom).

4. Conclusions and perspectives

In this paper, it has been shown that it is possible to predict the viscoelastic behavior described by internal variables under creep and cyclic loading with the PGD method by considering a globalization of the local models. This method allows describing all the different responses with respect to the relaxation times and the characteristic time of the load.

To highlight the potentiality of the method, different characteristic times have been investigated: the frequency of the loading cycle, the characteristic times of the viscoelastic behavior and the total duration of the simulation. In assessing the responses in different configurations, it has been showed that the PGD was able to reproduce both cyclic responses in the regime of moderate viscoelasticity and responses with fatigue–creep occurring when the characteristic times of the mechanical behavior spread over several decades and oversee the loading characteristic time.

Moreover, to apply the PGD, as the studied model is strongly coupled, a globalization of the local models has been considered. This strategy is known to be computationally expensive.

We have presented a way to decrease this computation time, which consists in decreasing the number of time steps to describe the internal variables depending on the different time scales. We finally have illustrated the performances of this strategy by comparing the computation time obtained with this strategy and with the PGD in the case of a same basis for all the considered variables (displacement and all the internal variables). The gain depends on the considered time scales and the number of internal variables. This work shows that the PGD combined with an adaptive time step could be efficiently used to predict the viscoelastic behavior combined with internal variables under cyclic fatigue by decreasing the computation time.

Within a realistic time distribution, 50 relaxation times as suggested by Cunat [7], the gain in time is promising (gain ratio of 4.8) when adapted time discretizations are combined with the globalization strategy within the PGD framework. The next step is to extend this procedure to 3D cases and to include the test of this method with more complex behaviors like nonlinear viscoelasticity. For these cases, Finite-Element simulations have already been done and will allow us to compare computation times with respect to 3D Finite-Element simulations.

References

[1] P. Germain, Q.S. Nguyen, P. Suquet, Continuum thermodynamics, J. Appl. Mech. 50 (1983) 1010–1020.
[2] J. Lemaître, J.-L. Chaboche, Mechanics of Solid Materials, Cambridge University Press, New York, 1990.

[3] G.-A. Maugin, Internal variables and dissipative structures, J. Non-Equilib. Thermodyn. 15 (1990) 173–192.
[4] D.G.B. Edelen, A.E. Green, N. Laws, Non local continuum mechanics, Arch. Ration. Mech. Anal. 43 (1971) 36–44.
[5] A.-C. Eringen, A unified theory of thermomechanical materials, Int. J. Eng. Sci. 4 (1966) 179–202.
[6] C. Cunat, A thermodynamic theory of relaxation based on a distribution of non-linear processes, J. Non-Cryst. Solids 131–133 (1) (1991) 196–199.
[7] C. Cunat, The DNLR approach and relaxation phenomena, part I – historical account and DNLR formalism, Mech. Time-Depend. Mater. 5 (2001) 39–65.
[8] W.H. Press, B.P. Flannery, S.A. Teukolsky, W.T. Vetterling, Numerical Recipes in Pascal, Cambridge University Press, Cambridge, 1989.
[9] A. Berrehili, Y. Nadot, S. Castagnet, J.-C. Grandidier, C. Dumas, Multiaxial fatigue criterion for polypropylene – automotive applications, Int. J. Fatigue 32 (8) (2010) 1389–1392.
[10] A. Chatterjee, An introduction to the proper orthogonal decomposition, Curr. Sci. 78 (7) (2000) 808–817.
[11] P. Ladevèze, The large time increment method for the analysis of structures with non-linear behaviour described by internal variables, C. R. Acad. Sci. Paris, Sér. II 309 (1989) 1095–1099.
[12] F. Comte, H. Maitournam, P. Burry, T.M.L. Nguyen, A direct method for the solution of evolution problems, C. R. Mecanique 334 (2006) 317–322.
[13] N. Relun, D. Néron, P.A. Boucard, A model reduction technique based on the PGD for elastic–viscoplastic computational analysis, Comput. Mech. 51 (2013) 83–92.
[14] D. Ryckelynck, D. Missoum Benziane, Multi-level a priori hyper-reduction of mechanical models involving internal variables, Comput. Methods Appl. Mech. Eng. 199 (2010) 1134–1142.
[15] A. Ammar, B. Mokdad, F. Chinesta, R. Keunings, A new family of solvers for some classes of multidimensional partial differential equations encountered in kinetic theory modeling of complex fluids, J. Non-Newton. Fluid Mech. 139 (2006) 153–176.
[16] A. Ammar, M. Normandin, F. Daim, D. Gonzales, E. Cueto, F. Chinesta, Non-incremental strategies based on separated representations: applications in computational rheology, Commun. Math. Sci. 8 (2010) 671–695.
[17] P. Ladevèze, A. Nouy, On a multiscale computational strategy with time and space homogenization for structural mechanics, Comput. Methods Appl. Mech. Eng. 192 (2003) 3061–3087.
[18] A. Nouy, A priori model reduction through Proper Generalized Decomposition for solving time-dependent partial differential equations, Comput. Methods Appl. Mech. Eng. 199 (2010) 1603–1626.
[19] A. Nouy, A generalized spectral decomposition technique to solve a class of linear stochastic partial differential equations, Comput. Methods Appl. Mech. Eng. 196 (2007) 4521–4537.
[20] A. Ammar, B. Mokdad, F. Chinesta, R. Keunings, A new family of solvers for some classes of multidimensional partial differential equations encountered in kinetic theory modeling of complex fluids – part II: transient simulation using space–time separated representations, J. Non-Newton. Fluid Mech. 144 (2007) 98–121.
[21] F. Chinesta, A. Ammar, E. Cueto, Proper generalized decomposition of multiscale models, Int. J. Numer. Methods Eng. 83 (2010) 1114–1132.
[22] F. Chinesta, P. Ladeveze, E. Cueto, A short review on model order reduction based on proper generalized decomposition, Arch. Comput. Methods Eng. 18 (2011) 395–404.
[23] F. Chinesta, A. Ammar, A. Leygue, R. Keunings, An overview of the proper generalized decomposition with application in computational rheology, J. Non-Newton. Fluid Mech. 166 (11) (2011) 578–592.
[24] E. Pruliere, F. Chinesta, A. Ammar, On the deterministic solution of multidimensional parametric models using the proper generalized decomposition, Math. Comput. Simul. 81 (4) (2010) 791–810.
[25] F. Chinesta, A. Leygue, F. Bordeu, J.V. Aguado, E. Cueto, D. Gonzales, I. Alfaro, A. Ammar, A. Huerta, PGD-based computational vademecum for efficient design, optimization and control, Arch. Comput. Methods Eng. 20 (1) (2013) 31–59.
[26] A. Ammar, F. Chinesta, E. Cueto, M. Doblaré, Proper generalized decomposition of time-multiscale models, Int. J. Numer. Methods Eng. 90 (2012) 569–596.
[27] D. Neron, P. Ladevèze, Proper generalized decomposition for multiscale and multiphysics problems, Arch. Comput. Methods Eng. 17 (4) (2010) 351–372.
[28] M. Hammoud, M. Beringhier, J.-C. Grandidier, Application of the proper generalized decomposition method to a viscoelastic mechanical problem with a large number of internal variables and a large spectrum of the relaxation times, in: M. Papadrakis, et al. (Eds.), Proc. 4th Coupled Problems Conf., Koos, Greece, 2011, pp. 570–577.
[29] S. André, Y. Meshaka, C. Cunat, Rheological constitutive equation of solids: a link between model based on irreversible thermodynamics and on fractional order derivative equations, Rheol. Acta 42 (2003) 500–515.
[30] M. Beringhier, M. Gueguen, J.-C. Grandidier, Solution of strongly coupled multiphysics problems using space–time separated representations – application to thermoviscoelasticity, Arch. Comput. Methods Eng. 17 (4) (2010) 393–401.